Front. Earth Sci. 2023, 17(4): 933–944
https://doi.org/10.1007/s11707-022-1055-5

RESEARCH ARTICLE

Alternating influences of the Westerlies and Indian Summer Monsoon on the hydroclimate of the source region of the Yarlung Tsangpo over past 4000 yr

Zhe SUN (✉)[1,2], Zirui HUANG[1], Kejia JI[2], Mingda WANG[2,4], Juzhi HOU (✉)[2,3]

1 Institute of Geography and Resources Science, Sichuan Normal University, Chengdu 610066, China
2 Group of Alpine Paleoecology and Human Adaptation (ALPHA), State Key Laboratory of Tibetan Plateau Earth System, Resources and Environment (TPESER), Institute of Tibetan Plateau Research, Chinese Academy of Sciences, Beijing 100101, China
3 CAS Center for Excellence in Tibetan Plateau Earth Sciences, Chinese Academy of Sciences (CAS), Beijing 100101, China
4 School of Geography, Liaoning Normal University, Dalian 116029, China

Abstract The Yarlung Tsangpo, the longest river in the southern Tibetan Plateau (TP), has attracted much research attention aimed at understanding the factors controlling its modern hydrology and possible future discharge in the context of ongoing climate change. However, partly due to the complex regional climatic background, no consistent conclusions have been reached, especially for its upper reaches. Paleohydrological reconstructions of the source region of the Yarlung Tsangpo can potentially improve our understanding of the history of humidity and its response to climatic variability. In this study, we used a 97 cm gravity core from Gongzhu Co to reconstruct the hydrology change during the late Holocene. The core was dated using AMS ^{14}C and Pb/Cs methods, and we used measurements of element contents (determined by high-resolution XRF scanning), grain size, IC/TOC, and magnetic susceptibility to reconstruct hydroclimatic changes in the source of the Yarlung Tsangpo watershed since ~4000 yr ago. Combined with a modern meteorological data set, we found that PC1 of the XRF data, the Ca/(Fe + Ti) ratio, and EM1 of the grain size data were indicative of changes in humidity. Our records demonstrate a wet interval during ~4–1.7 ka BP (ka = 1000 yr, BP represents years before 1950 AD), followed by a dry period during since ~1 ka BP. Comparison with independent regional paleoclimatic records revealed shifts in the dominant factors controlling humidity. The wet interval during ~4–1.7 ka BP was coeval with a strengthened Westerlies, implying a dominant moisture supply from northern high latitudes. However, the extremely low values of Ca/(Fe + Ti) ratio during ~4–2.5 ka BP indicate potential glacial freshwater source, which is corroborated by the concurrent high magnetic susceptibility values and increased grain size. The rapid drying trend during ~1.7–1 ka BP suggests a switch in moisture supply from the Westerlies to the Indian Summer Monsoon (ISM). We attribute the drought conditions after ~1 ka BP to a weakened ISM, although a Westerlies influence and the potential effect of high temperatures on evaporation cannot be excluded. We suggest that future hydroclimatic research in this region should attempt to distinguish the individual moisture contributions of the ISM and the Westerlies during the last millennium.

Keywords late Holocene, humidity changes, Westerlies, ISM, Yarluang Tsangpo

Received October 12, 2022; accepted December 21, 2022

E-mails: sunzhe@sicnu.edu.cn (Zhe SUN)
Houjz@itpcas.ac.cn (Juzhi HOU)

* Sun, Z. and Huang, Z. contributed equally to this work.

1 Introduction

The Tibetan Plateau (TP) has been called the ‘Asian Water Towers’ (Xu et al., 2008) because it is the source region of numerous major rivers, including the Yarlung Tsangpo (Brahmaputra), Indus, Ganges, Yellow, Yangtze, Mekong, and Salween, which are indispensable freshwater resources for East and South Asia. Additionally, the Yarlung Tsangpo valley is the most populated area in Tibet and therefore understanding its future status as a water resource against the background of ongoing climate change is of major social concern. Previous research on the Yarlung Tsangpo has utilized various hydrological models to project future changes in discharge; for example, Lutz et al. (2014) suggested that the discharge will increase until the middle of the present century and that precipitation is the most important driver

of this trend. However, Su et al. (2016) suggested that more than half of the runoff increase would be supplied by glacier meltwater, especially in the upper reaches. Wang et al. (2021) used a historical atmospheric circulation–precipitation relationship to constrain future modeled wet-season precipitation in the Yarlung Tsangpo watershed, and concluded that precipitation would make the dominant contribution to increased runoff in the future.

These different projections show that our understanding of the factors controlling the discharge of the Yarlung Tsangpo is limited, and therefore that there is a need for paleohydrological reconstructions of the Yarlung Tsangpo to help predict its future status. The climate of the TP is controlled mainly by the Indian Summer Monsoon (ISM) and the Westerlies, on seasonal, decadal, millennial, and orbital timescales (Schiemann et al., 2009; An et al., 2012; Zhu et al., 2015), and therefore variations of the ISM and the Westerlies are important for regulating the hydrological status of the 'Asian Water Towers' (Yao et al., 2022). The past variability of the ISM and Westerlies and their interplay have been addressed in numerous previous studies. In general, the ISM is assumed to have penetrated the entire TP since the early Holocene, based on stable isotope records from lacustrine sediments (Hou et al., 2017a) and cave deposits (Cai et al., 2012). Also, variations of the Westerlies have been suggested to be out-of-phase with those the ISM (Chen et al., 2008), with the Westerlies occasionally strengthening when the ISM weakened during the Holocene (Hou et al., 2017a). The Yarlung Tsangpo watershed is predominantly influenced by changes in the ISM, except for the source region (the Chema Yongdrung Glacier) where the role of the Westerlies must be considered. Chen et al. (2016) performed empirical orthogonal functions analysis (EOF) of a modern precipitation data set and found that rainfall across Tibet varied coherently during the last century, except for the south-western part of the region. Moreover, paleoclimatic reconstructions for the south-western TP and the adjacent regions are inconsistent with each other (Li et al., 2021). For example, studies of pollen assemblages and basin geomorphology, combined with multi-proxy records, from Tso Kar highlighted the dominant influence of the ISM on hydrological changes during the Holocene (Demske et al., 2009; Wünnemann et al., 2010), which was also demonstrated by records from the Tso Moriri in Ladakh (Leipe et al., 2014; Mishra et al., 2015). Additionally, Ma et al. (2014) showed that the climate of the south-western TP was hot and dry during the early Holocene and cold and dry during the late Holocene, which was attributed the to the Westerlies influence, whereas the influence of the ISM caused this region to be cold and wet during the middle Holocene. However, both the paleo-shoreline record of nearby Ngangla Ring Co (Hudson et al., 2015) and Baqan Co (Huth et al., 2015) indicated continuously decreasing lake levels during the Holocene that were attributed to the weakening of the ISM. In summary, the Holocene hydroclimatic evolution of the south-western TP and its response to external drivers remain unclear. The inconsistent results and conclusions obtained in previous studies may result from differences in the hydroclimatic sensitivity of the various proxies used, combined with the effects of local variations in moisture supply such as from glacial meltwater.

To address these issues, we obtained a multi-proxy data set from the late Holocene sediments of Gongzhu Co, near the source of the Yarlung Tsangpo in the south-western TP. Our specific objectives were: 1) to reconstruct the late Holocene paleohydrology of the source region of the Yarlung Tsangpo, and 2) to determine its principal drivers based on a comparison of our results with contemporary climate records.

2 Materials and methods

2.1 Study site

Gongzhu Co (30°35′–30°41′N; 82°02′–82°13′E, 4795 m above sea level, Fig. 1), is located within the south-western TP. The lake area is 66.2 km^2 and the watershed area is 849.8 km^2. It is a closed basin lake, fed by precipitation and by several rivers originating from Gangdisê Mountains to the east and north. Due to strong evaporation, the lake surface water is brackish with a salinity of 5.4 g/L (Wang and Dou, 1998). The surrounding vegetation is sparse and dominated by sedges. Exposed watershed lithologies are Triassic and Paleozoic clastic sediments and limestone (Ma, 2002). According to data from the nearest meteorological station at Pulan (30.28°N, 81.25°E; ~100 km to the south-west of Gongzhu Co, 3900 m above sea level), for 1973–2015 the mean annual precipitation was 158.7 mm, with 44% and 39% occurring during summer (Jun.–Sep.) and spring (Feb.–May), respectively (Fig. 1(c)), and the mean annual air temperature was 3.5°C.

2.2 Sediment sampling and radiometric dating

A 97 cm sediment downcore was retrieved from Gongzhu Co in August 2017, using a UWITEC gravity corer at a water depth of 22.4 m. The core was split vertically in the laboratory and the fresh sediment profile showed a transition from brown silt to black silt. One core half was used for the measurement of geochemical elements by high-resolution XRF scanning, and the other half was sliced at 0.5-cm intervals and the samples were freeze-dried for proxy measurements and radiometric dating. The age model for the top 20 cm of the core was established using the combination of ^{210}Pb and ^{137}Cs analyses, and AMS ^{14}C dating at 10 cm intervals was used for the interval of 30–90 cm. ^{210}Pb and ^{137}Cs activities were measured with ORTEC GWL Series High-

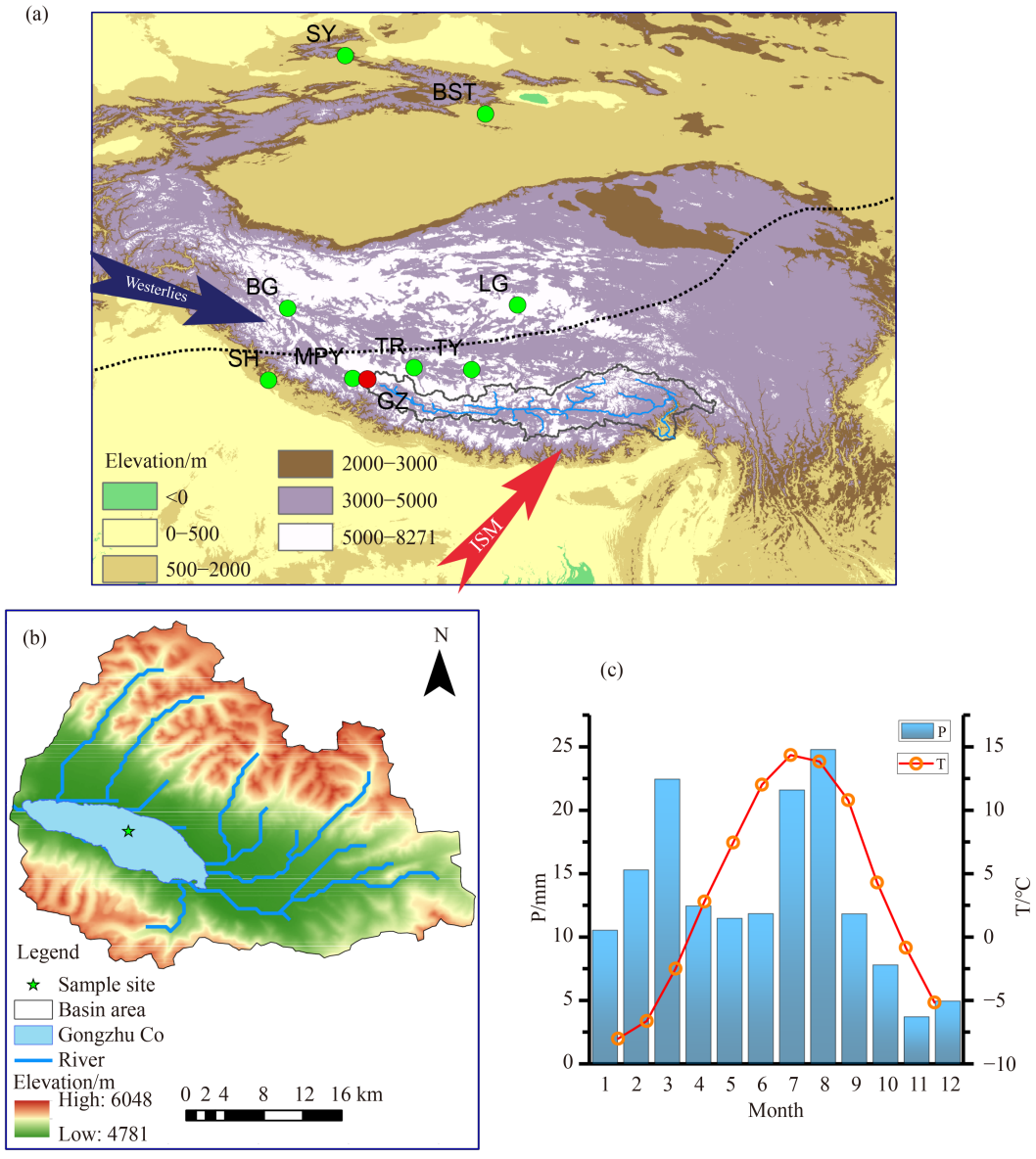

Fig. 1 (a) Locations of Gongzhu Co (red circle) and comparison sites referenced in the text (green circles): Lake Sayram (SY), Lake Bosten (BST), Bangong Co (BG), Sahiya cave (SH), Mapam Yumco (MPY), Taro Co (TR), Tangra Yumco (TY), Linggo Co (LG). The gray line represents the Yarlung Tsangpo watershed, the blue lines represent the Yarlung Tsangpo River, and the dotted line represents the northern modern boundary of the Asian Summer Monsoon region. (b) Enlarged map of the Gongzhu Co watershed based on a DEM. The sampling location is represented by a green star. (c) Monthly air temperature (red dotted curve) and precipitation (blue bars) at Pulan meteorological station for 1973–2015.

Purity Germanium (HPGe) Well Detectors at the Institute of Tibetan Plateau Research, Chinese Academy of Sciences (ITPCAS), and a total of seven AMS ^{14}C dates, based on the total organic matter content, were determined by Beta Analytic Inc. (Florida, USA). The final chronology was constructed using the *rbacon* package (Blaauw and Christen, 2011) implemented on the R platform.

2.3 XRF and magnetic susceptibility measurements

The relative abundances of geochemical elements were measured at a resolution of 0.2 mm using an ITRAX XRF core scanner at ITPCAS. The measurement settings were as follows: current 50 mA, voltage 30 kV, exposure time 10 s. The magnetic susceptibility (MS) at 4 mm resolution was measured after XRF measurements using a Bartington MS2E surface scanning sensor (Bartington, Oxford, UK) attached to the ITRAX XRF core scanner.

2.4 Grain size and IC (TOC) measurements

Approximately 200 mg of dry sample was treated sequentially with 20 ml of 30% H_2O_2 and 10 mL of 10%

HCl to remove organic matter and carbonates, respectively. The samples were then rinsed with deionized water and left standing overnight. After removing the supernatant, 10 mL of 0.05N $(NaPO_3)_6$ were added and the samples were subjected to ultrasonic vibration to promote dispersion. Grain size measurements were made with a Mastersizer 3000 laser grain-size analyzer with the measurement range of 0.01–3500 μm. The reported results are based on the average of three replicate measurements with the standard deviation < 5%. Parametric end- member analysis (EMMA) was used to extract information on source contributions, and was implemented with the Gen.Weilbull routine in the Matlab program provided by Paterson and Heslop (2015). This approach to the unmixing of sedimentary grain size data provides detailed information on subpopulations, which may be related to different sediment sources or source processes that can be appropriately unmixed into unimodal end-members.

The inorganic carbon (IC) and total carbon (TC) contents were measured using a Shimadzu TOC-VCPH analyzer. Approximately 150 mg of dry sample was combusted in oxygen at 950°C to determine the TC. The IC was determined from the evolved CO_2 after reacting dry samples with phosphoric acid at 200°C. Total organic carbon (TOC) was calculated as the difference between TC and IC.

3 Results

3.1 Chronology

The profile of $^{210}Pb_{ex}$ activity versus depth shows an exponentially decreasing trend and therefore we used the constant rate of supply (CRS) model (Appleby and Oldfield, 1978) to establish the chronology for the top 22 cm (Fig. 2(b)). The CRS results indicate an age of −18 ± 9 yr BP (equal to 1968 AD) for the depth of 9 cm where the ^{137}Cs activity is at a maximum (regarded as the 1963 AD maximum in atmospheric nuclear weapons testing), and therefore we regard the dating results as reliable. For the deeper section of the core (Table 1), the ^{14}C ages are generally in stratigraphic order, except for the sample from 50 cm depth; it is possible that this anomalous ^{14}C age is the result of a variable reservoir effect on the ^{14}C age of the sedimentary organic matter (Hou et al., 2012). To establish a reliable chronology for this interval we made a correction for the reservoir effect using the following steps. First, we extrapolated the

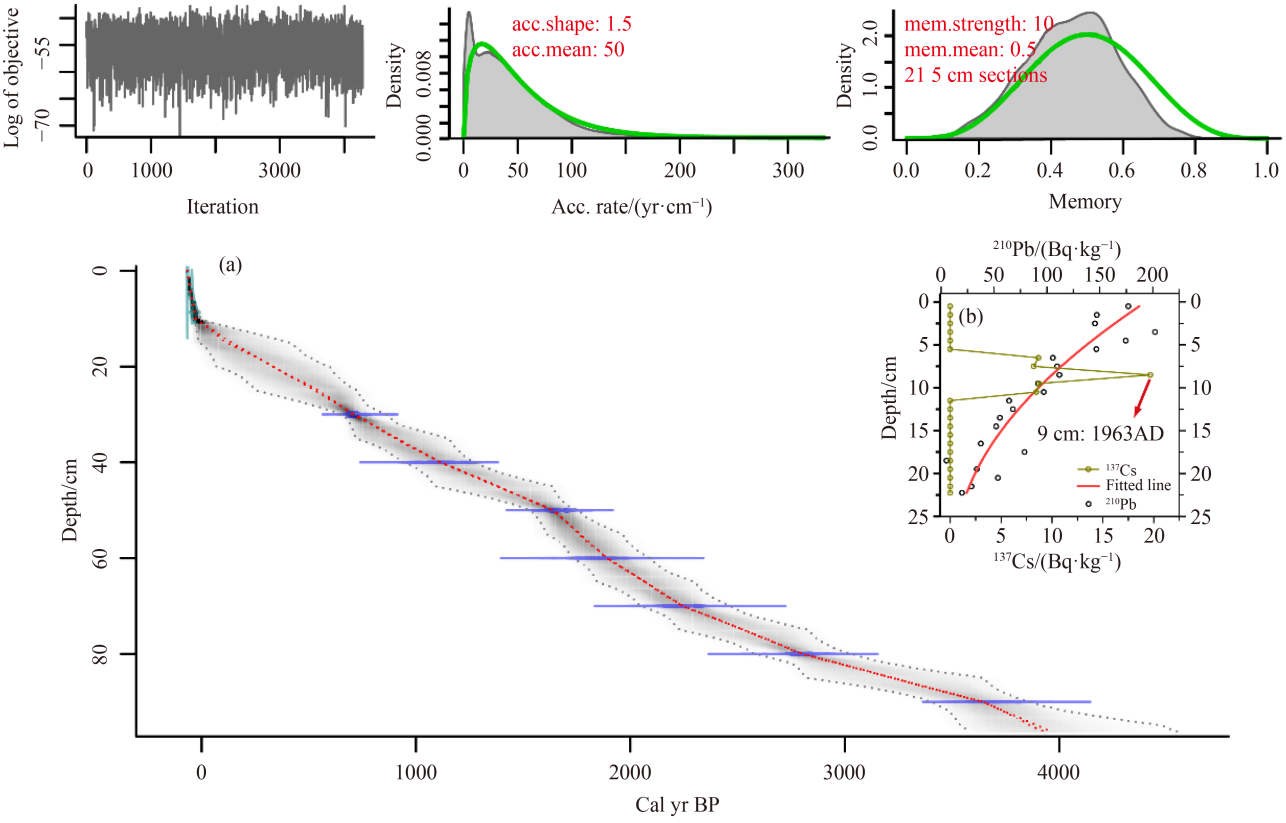

Fig. 2 (a) Age-depth model for the sediment core from Gongzhu Co. (b) The chronology of the top 20 cm is based on ^{210}Pb and ^{137}Cs ages (inset graph), and that of the lower part is based on seven ^{14}C ages based on bulk organic matter. The gray dotted line represents 95% confidence intervals, and the red dotted line represents the best-fit ages based on the weighted mean age for each depth interval.

Table 1 Radiocarbon ages and calibrated ages obtained using CALIB 8.1 for Gongzhu Co

Laboratory ID	Depth/cm	Material	^{14}C age/(yr BP)	Error/yr	RA* corrected ^{14}C age/(yr BP)	Cal age/(yr BP)	Cal age error/yr
Beta-624805	30	TOC	3660	30	800	706	18.5
Beta-635098	40	TOC	4050	30	1190	1116	61.5
Beta-635099	50	TOC	3570	30	1782	1645	22
Beta-624806	60	TOC	3710	30	1922	1818	77
Beta-635100	70	TOC	4030	30	2242	2210	57.5
Beta-635101	80	TOC	4470	30	2682	2800	48.5
Beta-624807	90	TOC	5230	30	3442	3675	58.5

* RA represents the reservoir age (2860 yr for the depth interval of 30–40 cm, and 1788 yr the reservoir age for the interval of 50–90 cm).

sediment ages based on the uppermost two ^{14}C ages to the depth dated to 1963 AD by the ^{210}Pb/^{137}Cs chronology, and used the difference of 2860 yr as the reservoir age for the interval of 30–40 cm. We then used this reservoir age to correct the top two ^{14}C ages and extrapolated the sediment ages based on the lower five ^{14}C ages to the depth of 40 cm, which gave the age of 2978 yr. The difference (1788 yr) between the extrapolated age and the reservoir-corrected age at the depth of 40 cm is regarded as the reservoir age for the interval of 50–90 cm. The final chronology (Fig. 2(a)) was established using the *rbacon* program (Blaauw and Christen, 2011). The age model shows that the 97 cm core spans the past ~4000 yr. It should be noted that the change in reservoir age at 1.7 ka BP is coeval with the clastic sediment influx (Fig. 5(g)). However, the stronger terrestrial input and the stable sediment accumulation rate before 1.7 ka BP cannot explain the change in reservoir age. We suspect that an environmental change from humid to dry conditions at 1.7 ka BP (see the subsequent discussion) resulted in a lower lake level. The reduction in the distance from the lake margin to the center of the lake may have caused the increased influx of old carbon from the watershed and thus to a larger reservoir effect.

3.2 XRF and magnetic susceptibility

A total of 7 elements (Ti, K, Si, Ca, Sr, Fe, Mn) were selected based on the criterion of CPS (counts per second) > 100, and the raw data were then normalized by the sum of incoherent and coherent counts (inc + coh) to minimize the effects of changes in grain size and in the contents of water and organic matter (Guyard et al., 2007). The element profiles can be roughly divided into three groups based on stratigraphic variability (Fig. S1). Type I: Ti, K, and Si show similar stratigraphic patterns, with relatively stable values and only minor fluctuations during ~4–1.7 ka BP. This is followed by rapid decreases during 1.7–1 ka BP, with low and relatively stable concentrations since ~1 ka BP. Type II: Ca and Sr concentrations were high during 2.5–1 ka BP compared with the preceding and subsequent intervals. Type III: Fe and Mn concentrations were high during ~4–2.5 ka BP, with a decreasing trend thereafter. Principal component analysis (PCA) was conducted to summarize the variance of the element contents. The first component (PC1) accounts for 55.1% of the total variance and all elements have positive loadings on this axis (Fig. 3).

The MS values range from 0.36 to 11.28 SI and show a similar stratigraphic pattern to that of Fe and Mn (Fig. S1). The only difference is that MS shows a decreasing trend during ~4–3 ka BP while Fe and Mn are relatively uniform.

3.3 Grain size and IC (TOC)

The median grain size (MZ) fluctuates between 8.5 μm and 40.9 μm with the mean of 14.9 μm (Fig. 4(b)). In detail, MZ increased from 10.9 μm to 25.3 μm during ~4–3 ka BP and decreased to 10 μm at ~2.4 ka BP. It then remained relatively uniform before increasing, with strong fluctuations, after ~1.2 ka. The EMMA yielded three end-members (Fig. 4(a)): The first end-member (EM1) represents fine silt with the modal size of 7.64 μm; the second end-member (EM2) represents medium silt

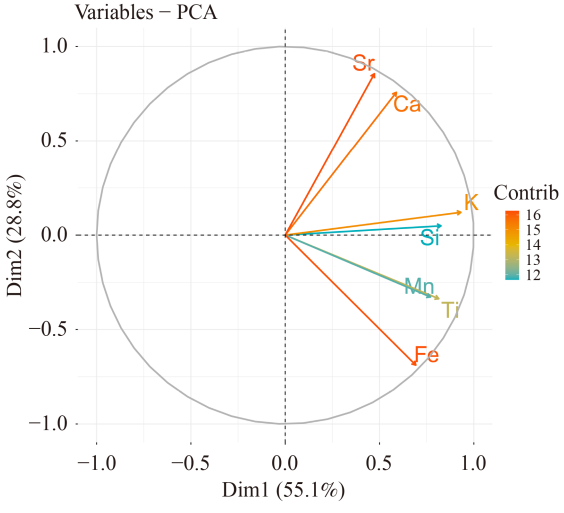

Fig. 3 Result of principal component analysis (PCA) of the XRF scanning data from Gongzhu Co.

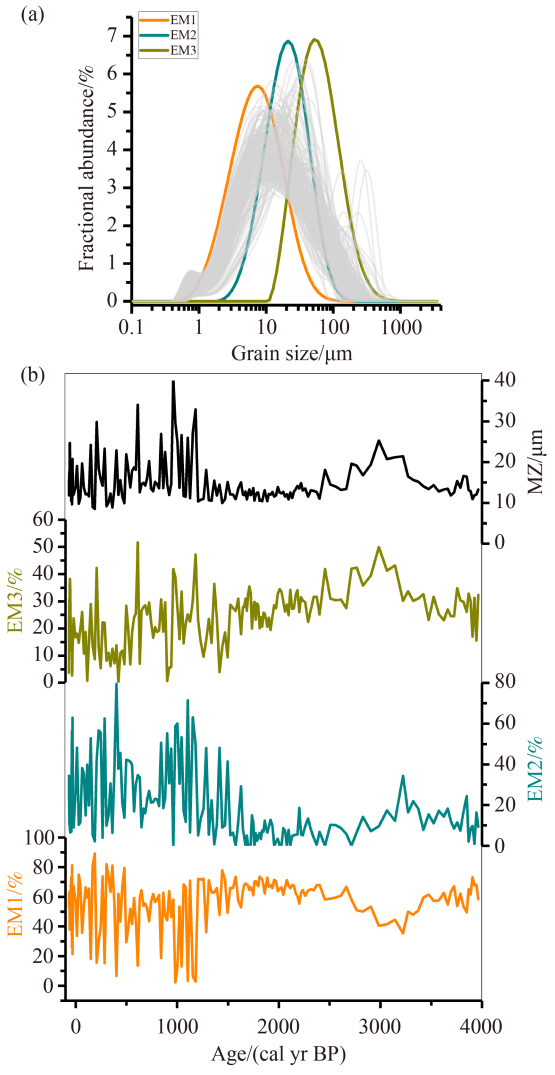

Fig. 4 (a) End-member loadings for the grain size data from Gongzhu Co downcore using the Gen.Weilbull method. The gray curves are the grain size distribution of subsamples. (b) Profile of median grain size and end-member scores for the sediment core from Gongzhu Co.

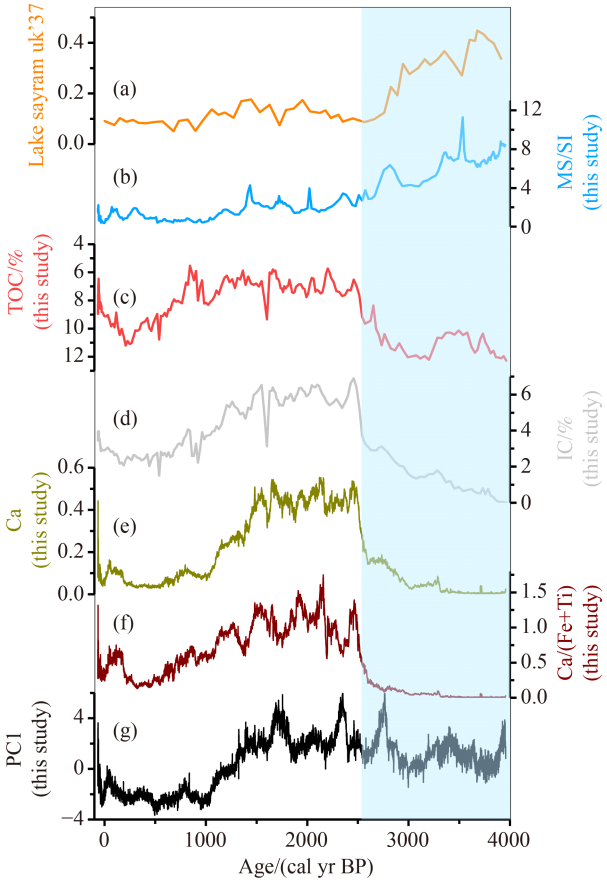

Fig. 5 Comparison of the proxy records from Gongzhu Co with summer temperature at Lake Sayram. (a) $U^{K'}_{37}$ record from Lake Sayram (Jiang et al., 2022). Profiles of various proxies from Gongzhu Co: (b) magnetic susceptibility (MS), (c) TOC content, (d) IC content, (e) calcium content, (f) Ca/(Fe + Ti) ratio, and (g) sample scores on PC1 of elements determined by scanning XRF.

with the modal size of 21.2 μm; and the third end-member (EM3) represents coarse silt with the modal size of 51.8 μm.

The TOC values vary between 5.52% and 12.27%, and the IC values vary between 0.01% and 6.9% (Figs. 5(c) and 5(d)). In general, the stratigraphic variations of IC are out of phase with those of TOC and in phase with those of Ca. A distinctive feature is the high content of IC during ~2.5–1.5 ka BP, with corresponding low TOC values continuing to ~1 ka BP.

4 Discussion

4.1 Hydroclimatic implications of the proxies

PC1 of the PCA of the XRF data represents 55.1% of the total variance. All elements have positive loadings on PC1, especially the lithogenic elements like Ti, K, and Si; these lithogenic elements generally reflect changes in the input of terrigenous debris from the watershed (Jin et al., 2006; Kylander et al., 2011; Lu et al., 2017). Gongzhu Co is mainly recharged by precipitation and river inputs and therefore we speculate that temporal changes in sample scores on PC1 should reflect changes in local precipitation and/or humidity. The lithogenic elements (e.g. Ti), however, could reflect fluctuations in eolian supply as well as precipitation changes, which would result in the opposite climatic interpretation (Hou et al., 2017b), and therefore additional evidence is needed to resolve this uncertainty. The changes in MS generally track those of the lithogenic elements, except for the high MS values during ~4–3 ka BP (Fig. S1). Since the MS is largely controlled by the type and concentration of detrital magnetic minerals (Snowball et al., 1999), this similarity suggests that the sample scores on PC1 reflect detrital influxes controlled by local precipitation. Moreover, due to the high resolution of the XRF scanning data, we can

directly compare the relationship between the PC1 scores with the precipitation data from Pulan meteorological station and with gridded reanalysis data. Both the rainfall data from Pulan station and from the CMFD data set (meteorological forcing data set for land process studies over China) (He et al., 2020) resemble the temporal variation of PC1 scores at Gongzhu Co (Fig. S2). This supports the conclusion that PC1 reflects precipitation. The stronger relationship for the CMFD data set than for the data from Pulan station may be because Pulan is ~100 km from the study site, and the CMFD data have a spatial resolution of 0.1°. Considering the complex effect of topography on precipitation in Tibet, the CMFD data set may be a more reliable indicator of changes in rainfall in the Gongzhu Co watershed. Therefore, we tentatively regard PC1 as an indicator of effective humidity (P/E) because the large temperature changes over the past few millennia may have modified the precipitation via strong evaporation. To sum up, we regard the temporal changes in the sample scores on PC1 of the XRF data set as a proxy of local humidity, with high values indicating wet conditions and vice versa.

The sedimentary carbonate content in closed basin lakes on the TP is influenced both by allogenic inputs and authigenic production (Cohen, 2003). The ratio of Ca to Ti + Fe + Al is usually used to reflect authigenic production (Mueller et al., 2009). Here, we simplify this to Ca/(Fe + Ti), since Al did not meet the reliability criterion for the XRF scanning data. Ca/(Fe + Ti) is strongly correlated with Ca (r = 0.9, p < 0.01, Figs. 5(e) and 5(f)), indicating that almost all the Ca-carbonate was precipitated within the lake. In addition, Ca/(Fe + Ti) is correlated with PC1 sample scores after 2.5 ka (r = 0.76, p < 0.01, Figs. 5(f) and 5(g)), which implies that authigenic carbonate precipitation was modulated by terrestrial inputs. This scenario was also reported at Lake Qinghai where the lake water has a much lower Ca^{2+} concentration than that of the inflowing rivers and groundwater, and therefore the carbonate precipitation balances the quantity of Ca^{2+} supplied to the lake by river water, which is related in turn to local humidity (An et al., 2012). This may also be the case at Gongzhu Co, although we cannot determine either Ca^{2+} or DIC was limited in the past. Like the PC1 scores, the Ca/(Fe + Ti) ratio also shows a similar pattern of variation to the precipitation (Fig. S2), which further supports the conclusion that Ca/(Fe + Ti) reflects humidity conditions. However, the relationship between PC1 and Ca/(Fe + Ti) was weak (r = 0.2, p < 0.01) during 4–2.5 ka BP, possibly because of the extremely low values of Ca/(Fe + Ti). The TOC content of lacustrine sediments is supplied by terrestrial inputs and aquatic production, and it is related to factors like temperature, precipitation, land cover, and lake level. Since the TOC is anti-correlated with IC, and the carbonate is suggested to be controlled by terrestrial inputs, the TOC at Gongzhu Co likely represents aquatic production which is sensitive to temperature changes (Mischke and Zhang, 2010). A pollen study of nearby Taro Co indicated dominance of steppe vegetation throughout the Holocene (Ma et al., 2014), and therefore we exclude vegetation change as a control on the sedimentary TOC. The antiphase relationship between TOC and precipitation suggests that increased rainfall lowers the production rate of aquatic organic matter, possibly because aquatic plants prefer a shallow water habitat. However, we lack bathymetry data for Gongzhu Co and thus we cannot corroborate this assumption. The temporal variations in TOC at Gongzhu Co since ~4 ka BP are comparable to those at the nearby site of Mapam Yumco (Zhu et al., 2019), which were also from aquatic origin and were interpreted to reflect temperature changes. Since Mapam Yumco and Gongzhu Co are only 40 km apart and are separated by an area of high, flat terrain, we infer that the interpretation of the TOC record at Mapam Yumco can also be applied to Gongzhu Co.

The EMMA of the grain size data resulted in three end-members, each of which are of potential paleoclimatic significance. EM1 represents the fine silt fraction (mode, 7.64 μm) the stratigraphic variation of which is like that of the lithogenic elements. Additionally, EM1 at Gongzhu Co is comparable to those at Hala lake and Donggi Cona (Dietze et al., 2012; Wang et al., 2015), which were interpreted as reflecting watershed runoff. We therefore conclude that EM1 is indicative of local humidity variations and hence lake level changes, because a higher lake level and the resulting deeper sedimentary environment promotes the accumulation of finer-grained sediments, and vice versa (Wang et al., 2019). EM2 (mode: 21.2 μm) and EM3 (mode: 51.8 μm) represent the medium and coarse silt fractions, respectively. According to Dietze et al. (2014), both EM2 and EM3 on the TP are indicative of a nearby dust source, with the difference being that EM2 may reflect dust remaining in longer-term suspension, while EM3 represents a near-surface suspension component related to the intermittent influence of Westerlies storms in winter and spring. Considering that the eolian dust in the upper Yarlung Tsangpo valley is mainly transported from nearby sources by the Westerlies (Ling et al., 2021), and the median grain size of the eolian dust in the valley is 42–50 μm (Jin et al., 2000), EM3 is suggested to reflect the Westerlies intensity. Note both the median grain size and sample scores on three EMs show pronounced oscillations during the last 1 kyr, which is not reproduced in the element variation. The possible reason is that the endogenous silicon related to diatom is responsible for this phenomenon (Liu et al., 2014). We take the Si/Ti ratio to represent the biosilicon (Brown et al., 2007; Kylander et al., 2011) and find it indeed shows relatively high variability during recent 1.2 ka (Fig. S4). In addition, this strong fluctuation of grain size may also be related to the local storm activities as reported in the

probability distribution function of eolian sediment ages in this region (Ling et al., 2020).

4.2 Hydrological variations at Gongzhu Co since 4 ka BP

From the foregoing we conclude that PC1 of the XRF data set, EM1 of the grain size data set, and the Ca/(Fe + Ti) ratio all reflect changes in local humidity. In the following discussion, we focus on the PC1 sample scores to infer changes in wetness, due the very high stratigraphic resolution of the XRF data. The inferred hydrological history of Gongzhu Co can be divided into the following two stages.

Stage I (4–1.7 ka BP): the PC1 scores are high during this interval (Fig. 5(g)), indicating relatively wet conditions, which were also recorded at Nam Co (Chen et al., 2017), Linggo Co (Pan et al., 2012), and Hurleg lake (He et al., 2016). However, the Ca/(Fe + Ti) ratios were extremely low during 4–2.5 ka BP (Fig. 5(f)), and since Ca/(Fe + Ti) is interpreted as authigenic carbonate precipitation controlled by terrestrial inputs, such low values denote a dry interval rather than humid conditions. In contrast, the EM1 scores indicate a high lake level during ~4–1.7 ka BP (Fig. 4), supporting the PC1 scores. A possible explanation is the increased influx of glacial meltwater to the lake during ~4–2.5 ka BP, because cold freshwater would depress the saturability of carbonate (Nishimura et al., 2014). A similar scenario was reported for Dagze Co, where an increase in lake level during ~3.4–2.2 ka BP was attributed to the combination of increased rainfall and glacial meltwater influx (Liu et al., 2022). Support for this inference is provided by the MS record which shows a similar pattern to that of the PC1 scores, with higher MS values during ~4–2.5 ka BP (Fig. 5(b)), indicating the increased influx of magnetic minerals, possibly because of the effect of glacial meltwater on watershed runoff (Li et al., 2021). Increased glacial meltwater influx is also supported by the increase in the median grain size (Fig. 4(b)). A contemporary warm period, validated by newly updated alkenone-based summer temperature data from Lake Sayram (Fig. 5(a)) (Jiang et al., 2022), together with the TOC record from Gongzhu Co (Fig. 5(c)), provides additional support for this meltwater hypothesis. Although Sayram lake is located within Xinjiang Uygur Autonomous Region in north-west China, distant from our study site, we used the NCEP-NCAR Reanalysis data to perform EOF analysis and produced coherent temperature changes during spring through summer (Fig. S3), which means that this inferred warm period may have been spatially extensive. To sum up, a wet period during ~4–1.7 ka BP is recorded by our multiproxy data set, but increased meltwater influx may have been important during ~4–2.5 ka BP.

Stage II (1.7 ka BP to the present): the multiproxy data indicate a drying trend during this interval. The humidity rapidly decreased from 1.7 ka BP onwards and reached a low level at ~1 ka BP, which is supported by the Ca/(Fe + Ti) record as well (Fig. 5(f)). EM1 of the grain size data indicates a similar pattern, although there are large fluctuations after ~1.2 ka BP (Fig. 4), which may be related to local storms, as reported by Ling et al. (2020); this is because the effects of strong winds are reinforced by a canyon effect which likely affects the lake surface and modifies the grain size distributions prior to deposition. Nevertheless, the EM1 samples scores are relatively low after ~1 ka, indicating a low lake level and dry conditions.

4.3 Combined effects of the ISM and the Westerlies on the late Holocene paleohydrology of Gongzhu Co

Our data reveal a relatively stable wet period at Gongzhu Co during ~4–1.7 ka BP, followed by a sustained dry period. However, this scenario is not replicated in comparable studies from the surrounding region. For example, the IC content at the nearest site of Mapam Yumco was suggested to indicate wet conditions followed by a continuous aridification trend after ~3 ka BP, which was attributed to the weakening of the ISM in the late Holocene (Zhu et al., 2019). The oxygen isotopic composition of sedimentary carbonate at Zabuye Lake indicated an enrichment trend after ~5 ka BP, which was also ascribed to the weakening of the ISM (Wang et al., 2002). Sample scores on PC1 of pollen data from Taro Co also indicate a persistent drying trend after ~3 ka BP (Ma et al., 2014). These inconsistencies may be caused by variations in moisture conditions and specific local responses to large-scale climate change. The Mapam Yumco is less than 50 km from Gongzhu Co, but shows distinct humidity change in the late Holocene. We suggest that the different hydroclimatic patterns may be the result of the effect of glacial meltwater influx. This is because Mapam Yumco is recharged by an enormous volume of meltwater from the western Himalayan Mountains, while no modern glacier is present in the Gongzhu Co Basin and it is only recharged by seasonal meltwater in spring and summer. Direct evidence for this inference is provided by the salinities of the two lakes: the salinity of Gongzhu Co (5.4 g/L) is more than ten times that of Mapam Yumco (0.45 g/L). The extremely low values (near zero) of the sedimentary IC content at Mapam Yumco during the early to middle Holocene, and the increase after ~3 ka BP, can be attributed to the gradually decreasing summer temperature (Li et al., 2021).

To evaluate the effect of atmospheric circulation on the hydrological conditions at Gongzhu Co we compared our data with published ISM records reconstructed from cave and lake sediments (Fig. 6). The interval of stable wet conditions at Gongzhu Co during ~4–1.7 ka BP is not replicated in those records. The carbon isotope records from Bangong Co (Hou et al., 2017a) and Tangra Yumco (Kasper et al., 2021) document an enrichment trend after

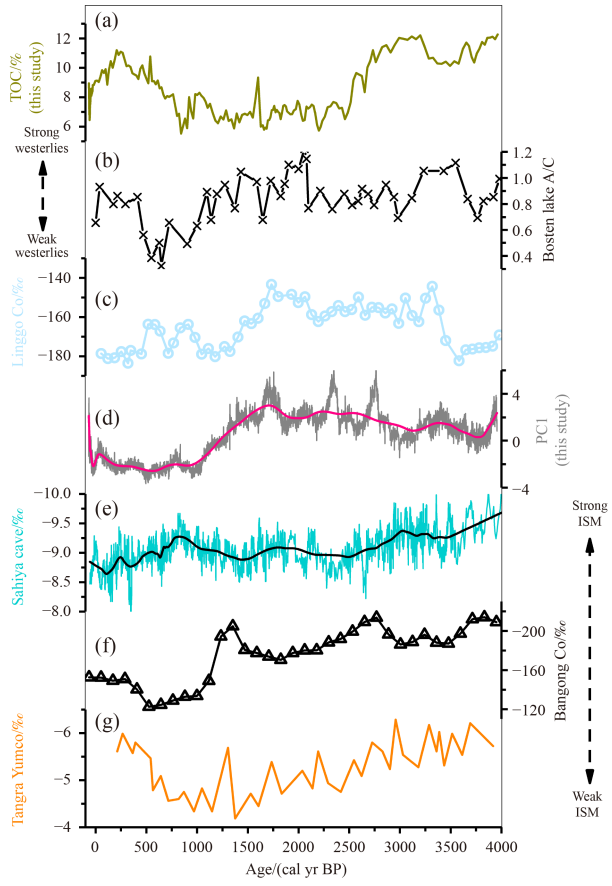

Fig. 6 Comparison of hydrological variations at Gongzhu Co with paleoclimatic records from other sites. (a) TOC content at Gongzhu Co. (b) A/C pollen ratio from Lake Bosten (Huang et al., 2009). (c) δD record from Linggo Co (Hou et al., 2017a). (d) Sample scores on PC1 of the scanning XRF data from Gongzhu Co. The red line represents the result of LOWESS smoothing with 0.1 window width. (e) $\delta^{18}O$ record from Sahiya cave (Kathayat et al., 2017). The black line represents the result of LOESS smoothing with 0.1 window width. (f) δD record from Bangong Co (Hou et al., 2017a). (g) $\delta^{18}O$ record from Tangra Yumco (Kasper et al., 2021).

~4 ka, followed by a depletion trend since ~1 ka BP (Figs. 6(f) and 6(g)). Moreover, the $\delta^{18}O$ record of Sahiya cave, which was interpreted to be regulated by monsoonal rainfall amount (Kathayat et al., 2017), shows almost the opposite pattern of variation to our data, especially after ~3 ka BP (Figs. 6(d) and 6(e)). Therefore, we conclude that ISM variability was not the major control of humidity conditions in the Gongzhu Co watershed. The bimodal distribution of modern seasonal precipitation (Fig. 1(c)) indicates that the Westerlies was an additional important moisture source. The variation of the *Artemisia*/Chenopodiaceae (A/C) pollen ratio from Bosten Lake (Huang et al., 2009) (Fig. 6(b)), which reflects changes in Westerlies-derived moisture, resembles our multiproxy records from Gongzhu Co. Moreover, the δD record of Linggo Co (Hou et al., 2017a) (Fig. 6(c)) in the north-central TP and an ice core $\delta^{18}O$ record from the Western Belukha Plateau (Aizen et al., 2016) indicate a strengthening of the Westerlies during ~3.5–1.7 ka BP, which is consistent with the stable wet period evident in our records. Together with the inference that glacier meltwater influx was responsible for the extremely low Ca/(Fe + Ti) ratios during ~4–2.5 ka BP, we suggest that the relatively wet period during ~4–1.7 ka BP was the result of a Westerlies moisture supply combined with local meltwater input. Subsequently, our records suggest a rapid transition from humid to dry conditions during ~1.7–1 ka BP, which agrees with the inferred shift from Westerlies-derived to ISM-derived moisture at Linggo Co δD (Fig. 6(c)). Regarding the dry interval after ~1 ka BP, the $\delta^{18}O$ record from Sahiya cave (Fig. 6(e)) shows a continuous decrease in summer rainfall. A weak ISM was also recorded at Bangong Co (Fig. 6(f)), which was likely responsible for the dry conditions indicated by our records. The $\delta^{18}O$ depletion observed at Bangong Co since ~0.5 ka BP may be the result of the closure of the lake (Gasse et al., 1996). In contrast, the pollen A/C ratio at Bosten Lake in Xinjiang decreased after ~1 ka BP and re-increased after ~0.5 ka BP (Fig. 6(b)), which suggests a complex pattern of changes in the Westerlies which may partly explain the dry conditions during ~1–0.5 ka BP. Additionally, the concurrent increase in the TOC content at Gongzhu Co (Fig. 6(a)) suggests the strengthening of temperature, which may also have contributed to the evaporation and aridification.

To sum up, comparison of the paleohydrological record from Gongzhu Co with independent paleoclimate records from adjacent area suggests that during the last ~4000 years the moisture supply at Yarlung Tsangpo was modulated by the combined effects of the ISM and the Westerlies. An extended wet period during ~4–1.7 ka BP was caused by the strengthened moisture supply by the Westerlies, while glacial meltwater may have been another major source during ~4–2.5 ka BP. The subsequent dry interval was mainly caused by the weakened ISM.

5 Summary

We have used a multi-proxy data set (elements determined by XRF scanning, grain size, and IC (TOC) content) from Gongzhu Co, south-western TP, in the source area of the Yarlung Tsangpo, to reconstruct changes in the hydrological conditions and their influencing factors during the last ~4000 years. The results suggest an interval of wet conditions during ~4–1.7 ka BP, followed by rapid aridification during ~1.7–1 ka BP., which was maintained after ~1 ka BP. We conclude that the strengthening of the Westerlies was the cause of this multi-millennial-scale wet interval, and that glacial meltwater may have an important additional contributor factor during ~4–2.5 ka BP. The drying trend after ~1 ka BP was likely related to a weakened ISM,

although the influences of the Westerlies and temperature-driven evaporation cannot be excluded. In future research, efforts should be made to develop proxy indicators that reflect hydrological and climatic variations in the same core, with the objective of distinguishing the moisture contributions of different atmospheric circulations during the last millennium.

Acknowledgments The work was financially supported by the National Natural Science Foundation of China (Grant No. 42025103), Basic Science Center for Tibetan Plateau Earth System (BSCTPES, NSFC project No. 41988101), and the Second Tibetan Plateau Scientific Expedition and Research program (No. 2019QZKK0601), as well as the Scientific Research Funding of Sichuan Normal University.

Data availability statement The data that support the findings of this study are available on request from the corresponding author. The data are not publicly available due to privacy or ethical restrictions.

Competing interests The authors declare that they have no competing interests.

References

Aizen E M, Aizen V B, Takeuchi N, Mayewski P A, Grigholm B, Joswiak D R, Nikitin S A, Fujita K, Nakawo M, Zapf A, Schwikowski M (2016). Abrupt and moderate climate changes in the mid-latitudes of Asia during the Holocene. J Glaciol, 62(233): 411–439

An Z, Colman S M, Zhou W, Li X, Brown E T, Jull A J T, Cai Y, Huang Y, Lu X, Chang H, Song Y, Sun Y, Xu H, Liu W, Jin Z, Liu X, Cheng P, Liu Y, Ai L, Li X, Liu X, Yan L, Shi Z, Wang X, Wu F, Qiang X, Dong J, Lu F, Xu X (2012). Interplay between the Westerlies and Asian monsoon recorded in Lake Qinghai sediments since 32 ka. Sci Rep, 2(1): 619

Appleby P G, Oldfield F (1978). The calculation of lead-210 dates assuming a constant rate of supply of unsupported ^{210}Pb to the sediment. Catena, 5(1): 1–8

Blaauw M, Christen J A (2011). Flexible paleoclimate age-depth models using an autoregressive gamma process. Bayesian Anal, 6(3): 457–474

Brown E T, Johnson T C, Scholz C A, Cohen A S, King J W (2007). Abrupt change in tropical African climate linked to the bipolar seesaw over the past 55000 years. Geophys Res Lett, 34(20): L20702

Cai Y J, Zhang H W, Cheng H, An Z S, Edwards R L, Wang X F, Tan L C, Liang F Y, Wang J, Kelly M (2012). The Holocene Indian monsoon variability over the southern Tibetan Plateau and its teleconnections. Earth Planet Sci Lett, 335–336: 135–144

Chen F H, Yu Z C, Yang M L, Ito E, Wang S M, Madsen D B, Huang X Z, Zhao Y, Sato T, Birks H J B, Boomer I, Chen J H, An C B, Wünnemann B (2008). Holocene moisture evolution in arid central Asia and its out-of-phase relationship with Asian monsoon history. Quat Sci Rev, 27(3–4): 351–364

Chen F, Feng J L, Hu H P, Zhang J F, Gao S P, Liu X M (2017). Potential forcing mechanisms of Holocene lake-level changes at Nam Co, Tibetan Plateau: inferred from the stable isotopic composition of shells of the gastropod Radix. Holocene, 27(4): 594–604

Chen J H, Rao Z G, Liu J B, Huang W, Feng S, Dong G H, Hu Y, Xu Q H, Chen F H (2016). On the timing of the East Asian summer monsoon maximum during the Holocene–does the speleothem oxygen isotope record reflect monsoon rainfall variability? Sci China Earth Sci, 59(12): 2328–2338

Cohen A S (2003). Paleolimnology: the History and Evolution of Lake Systems. New York: Oxford University Press

Demske D, Tarasov P E, Wunnemann B, Riedel F (2009). Late glacial and Holocene vegetation, Indian monsoon and westerly circulation in the Trans-Himalaya recorded in the lacustrine pollen sequence from Tso Kar, Ladakh, NW India. Palaeogeogr Palaeoclimatol Palaeoecol, 279(3–4): 172–185

Dietze E, Hartmann K, Diekmann B, Ijmker J, Lehmkuhl F, Opitz S, Stauch G, Wünnemann B, Borchers A (2012). An end-member algorithm for deciphering modern detrital processes from lake sediments of Lake Donggi Cona, NE Tibetan Plateau, China. Sediment Geol, 243–244: 169–180

Dietze E, Maussion F, Ahlborn M, Diekmann B, Hartmann K, Henkel K, Kasper T, Lockot G, Opitz S, Haberzettl T (2014). Sediment transport processes across the Tibetan Plateau inferred from robust grain-size end members in lake sediments. Clim Past, 10(1): 91–106

Gasse F, Fontes J C, VanCampo E, Wei K (1996). Holocene environmental changes in Bangong Co basin (western Tibet). 4. Discussion and conclusions. Palaeogeogr Palaeoclimatol Palaeoecol, 120(1–2): 79–92

Guyard H, Chapron E, St-Onge G, Anselmetti F S, Arnaud F, Magand O, Francus P, Melieres M A (2007). High-altitude varve records of abrupt environmental changes and mining activity over the last 4000 years in the Western French Alps (Lake Bramant, Grandes Rousses Massif). Quat Sci Rev, 26(19–21): 2644–2660

He J, Yang K, Tang W, Lu H, Qin J, Chen Y, Li X (2020). The first high-resolution meteorological forcing dataset for land process studies over China. Sci Data, 7(1): 25

He Y X, Zhao C, Liu Z H, Wang H Y, Liu W G, Yu Z C, Zhao Y, Ito E (2016). Holocene climate controls on water isotopic variations on the northeastern Tibetan Plateau. Chem Geol, 440: 239–247

Hou J Z, D'Andrea W J, Liu Z H (2012). The influence of C-14 reservoir age on interpretation of paleolimnological records from the Tibetan Plateau. Quat Sci Rev, 48: 67–79

Hou J Z, D'Andrea W J, Wang M D, He Y, Liang J (2017a). Influence of the Indian monsoon and the subtropical jet on climate change on the Tibetan Plateau since the late Pleistocene. Quat Sci Rev, 163: 84–94

Hou J Z, Tian Q, Liang J, Wang M D, He Y (2017b). Climatic implications of hydrologic changes in two lake catchments on the central Tibetan Plateau since the last glacial. J Paleolimnol, 58(2): 257–273

Huang X Z, Chen F H, Fan Y X, Yang M L (2009). Dry late-glacial and early Holocene climate in arid central Asia indicated by lithological and palynological evidence from Bosten Lake, China. Quat Int, 194(1–2): 19–27

Hudson A M, Quade J, Huth T E, Lei G L, Cheng H, Edwards L R, Olsen J W, Zhang H C (2015). Lake level reconstruction for

12.8–2.3 ka of the Ngangla Ring Tso closed-basin lake system, southwest Tibetan Plateau. Quat Res, 83(1): 66–79

Huth T, Hudson A M, Quade J, Lei G L, Zhang H C (2015). Constraints on paleoclimate from 11.5 to 5.0 ka from shoreline dating and hydrologic budget modeling of Baqan Tso, southwestern Tibetan Plateau. Quat Res, 83(1): 80–93

Jiang Q, Meng B, Wang Z, Qian P, Zheng J, Jiang J, Zhao C, Hou J, Dong G, Shen J, Liu W, Liu Z, Chen F (2022). Exceptional terrestrial warmth around 4200–2800 years ago in northwest China. Sci Bull (Beijing), 67(4): 427–436

Jin H L, Dong G R, Zhang C L (2000). Deposition features and causes of loess in Yarlung Zangbo River Valley area . J Desert Res, 20: 14–19 (in Chinese)

Jin Z D, Li F C, Cao J J, Wang S M, Yu J M (2006). Geochemistry of Daihai Lake sediments, Inner Mongolia, north China: implications for provenance, sedimentary sorting, and catchment weathering. Geomorphology, 80(3–4): 147–163

Kasper T, Wang J B, Schwalb A, Daut G, Plessen B, Zhu L P, Mausbacher R, Haberzettl T (2021). Precipitation dynamics on the Tibetan Plateau during the Late Quaternary–Hydroclimatic sedimentary proxies versus lake level variability. Global Planet Change, 205: 103594

Kathayat G, Cheng H, Sinha A, Yi L, Li X, Zhang H, Li H, Ning Y, Edwards R L (2017). The Indian monsoon variability and civilization changes in the Indian subcontinent. Sci Adv, 3(12): e1701296

Kylander M E, Ampel L, Wohlfarth B, Veres D (2011). High-resolution X-ray fluorescence core scanning analysis of Les Echets (France) sedimentary sequence: new insights from chemical proxies. J Quaternary Sci, 26(1): 109–117

Leipe C, Demske D, Tarasov P E (2014). A Holocene pollen record from the northwestern Himalayan lake Tso Moriri: implications for palaeoclimatic and archaeological research. Quat Int, 348: 93–112

Li C G, Wang M D, Liu W G, Lee S Y, Chen F H, Hou J Z (2021). Quantitative estimates of Holocene glacier meltwater variations on the Western Tibetan Plateau. Earth Planet Sci Lett, 559: 116766

Li X M, Yan H, Fan B W, Zhang C G, Xing W (2021). Climatic changes during the last two millennia on the southern Tibetan Plateau based on lake sediment and its forcing mechanisms. J Xinyang Normal U (Nat Sci Ed), 34(4): 584–588

Ling Z Y, Li J S, Jin J H, Wang J P, Kong F C, Chen L (2021). Geochemical characteristics and provenance of aeolian sediments in the Yarlung Tsangpo valley, southern Tibetan Plateau. Environ Earth Sci, 80(18): 623

Ling Z Y, Yang S L, Wang X, Wang J P, Xia D S, Chen F H (2020). Spatial-temporal differentiation of eolian sediments in the Yarlung Tsangpo catchment, Tibetan Plateau, and response to global climate change since the Last Glaciation. Geomorphology, 357: 107104

Liu B, Xu H, Lan J H, Sheng E G, Che S, Zhou X Y (2014). Biogenic silica contents of Lake Qinghai sediments and its environmental significance. Front Earth Sci, 8(4): 573–581

Liu X J, Wang Y X, Miao X D, Ou X J, Zheng C Y, Xu Y T, Lai Z P (2022). Holocene lake level variations of Dagze Co in central Tibetan Plateau revealed by OSL dates on palaeoshorelines. Catena, 219: 106645

Lu Y B, Fritz S C, Stone J R, Krause T R, Whitlock C, Brown E T, Benes J V (2017). Trends in catchment processes and lake evolution during the late-glacial and early- to mid-Holocene inferred from high-resolution XRF data in the Yellowstone region. J Paleolimnol, 58(4): 551–569

Lutz A F, Immerzeel W W, Shrestha A B, Bierkens M F P (2014). Consistent increase in High Asia's runoff due to increasing glacier melt and precipitation. Nat Clim Chang, 4(7): 587–592

Ma L F (2002) Gological Atlas of China. Beijing: Geology Press (in Chinese)

Ma Q F, Zhu L P, Lu X M, Guo Y, Ju J T, Wang J B, Wang Y, Tang L Y (2014). Pollen-inferred Holocene vegetation and climate histories in Taro Co, southwestern Tibetan Plateau. Chin Sci Bull, 59(31): 4101–4114

Mischke S, Zhang C J (2010). Holocene cold events on the Tibetan Plateau. Global Planet Change, 72(3): 155–163

Mishra P K, Anoop A, Schettler G, Prasad S, Jehangir A, Menzel P, Naumann R, Yousuf A R, Basavaiah N, Deenadayalan K, Wiesner M G, Gaye B (2015). Reconstructed late Quaternary hydrological changes from Lake Tso Moriri, NW Himalaya. Quat Int, 371: 76–86

Mueller A D, Islebe G A, Hillesheim M B, Grzesik D A, Anselmetti F S, Ariztegui D, Brenner M, Curtis J H, Hodell D A, Venz K A (2009). Climate drying and associated forest decline in the lowlands of northern Guatemala during the late Holocene. Quat Res, 71(2): 133–141

Nishimura M, Matsunaka T, Morita Y, Watanabe T, Nakamura T, Zhu L P, Nara F W, Imai A, Izutsu Y, Hasuike K (2014). Paleoclimatic changes on the southern Tibetan Plateau over the past 19000 years recorded in Lake Pumoyum Co, and their implications for the southwest monsoon evolution. Palaeogeogr Palaeoclimatol Palaeoecol, 396: 75–92

Pan B L, Yi C L, Jiang T, Dong G C, Hu G, Jin Y (2012). Holocene lake-level changes of Linggo Co in central Tibet. Quat Geochronol, 10: 117–122

Paterson G A, Heslop D (2015). New methods for unmixing sediment grain size data. Geochem Geophys Geosyst, 16(12): 4494–4506

Schiemann R, Lüthi D, Schär C (2009). Seasonality and interannual variability of the westerly jet in the Tibetan Plateau region. J Clim, 22(11): 2940–2957

Snowball I, Sandgren P, Petterson G (1999). The mineral magnetic properties of an annually laminated Holocene lake-sediment sequence in northern Sweden. Holocene, 9(3): 353–362

Su F, Zhang L, Ou T, Chen D, Yao T, Tong K, Qi Y (2016). Hydrological response to future climate changes for the major upstream river basins in the Tibetan Plateau. Global Planet Change, 136: 82–95

Wang C, Wang H L, Song G, Zheng M P (2019). Grain size of surface sediments in Selin Co (central Tibet) linked to water depth and offshore distance. J Paleolimnol, 61(2): 217–229

Wang R L, Scarpitta S C, Zhang S C, Zheng M P (2002). Later Pleistocene/Holocene climate conditions of Qinghai–Xizhang Plateau (Tibet) based on carbon and oxygen stable isotopes of Zabuye Lake sediments. Earth Planet Sci Lett, 203(1): 461–477

Wang R, Zhang Y Z, Wünnemann B, Biskaborn B K, Yin H, Xia F, Zhou L F, Diekmann B (2015). Linkages between Quaternary

climate change and sedimentary processes in Hala Lake, northern Tibetan Plateau, China. J Asian Earth Sci, 107: 140–150

Wang S M, Dou H S (1998). Lake in China. Beijing: Science Press (in Chinese)

Wang T, Zhao Y T, Xu C Y, Ciais P, Liu D, Yang H, Piao S L, Yao T D (2021). Atmospheric dynamic constraints on Tibetan Plateau freshwater under Paris climate targets. Nat Clim Chang, 11(3): 219–225

Wünnemann B, Demske D, Tarasov P, Kotlia B S, Reinhardt C, Bloemendal J, Diekmann B, Hartmann K, Krois J, Riedel F, Arya N (2010). Hydrological evolution during the last 15 kyr in the Tso Kar lake basin (Ladakh, India), derived from geomorphological, sedimentological and palynological records. Quat Sci Rev, 29(9–10): 1138–1155

Xu X D, Lu C G, Shi X H, Gao S T (2008). World water tower: an atmospheric perspective. Geophys Res Lett, 35(20): L20815

Yao T D, Bolch T, Chen D L, Gao J, Immerzeel W, Piao S L, Su F G, Thompson L, Wada Y, Wang L, Wang T, Wu G J, Xu B Q, Yang W, Zhang G Q, Zhao P (2022). The imbalance of the Asian water tower. Nat Rev Earth Environ, 3(10): 618–632

Zhu L, Lü X, Wang J, Peng P, Kasper T, Daut G, Haberzettl T, Frenzel P, Li Q, Yang R, Schwalb A, Mäusbacher R (2015). Climate change on the Tibetan Plateau in response to shifting atmospheric circulation since the LGM. Sci Rep, 5(1): 13318

Zhu S H, Zhu L P, Wang J B, Ju J T, Ma Q F, Chen H, Xu T, Kai J L (2019). Environmental changes reflected by core sediments since late glacial in Mapam Yumco, southwest Tibet of China. Quatern Sci, 39: 602–614 (in Chinese)